COBEM 2023 27TH INTERNATIONAL CONGRESS OF MECHANICAL ENGENEERING

ABCM Brazilian Society of Mechanical Sciences and Engineering
27th ABCM International Congress of Mechanical Engineering
December 04-08, 2023, Florianópolis-SC, Brazil

COB-2023-1244
INFLUENCE OF THERMAL CONTRAST DURING DYNAMIC THERMOGRAPHY ON A DEEP-LEARNING-BASED ESTIMATION OF BREAST TUMOUR PARAMETERS

Mateus Felipe Benicio Moraes[1]
Tarcio Cardoso Barros[2]
Alisson Augusto Azevedo Figueiredo[1,2]
[1]Federal Institute of Maranhão, Av. Getúlio Vargas, 04 - Monte Castelo, São Luís - MA, 65030-005
[2]State University of Maranhão, Av. Lourenço Vieira da Silva, 1000 - Jardim São Cristovão, São Luís - MA, 65055-310

mateusmoraes@acad.ifma.edu.br
tarciobarros1@aluno.uema.br
alissonfigueiredo@professor.uema.br

Abstract. *Thermography is a low-cost and non-invasive imaging method that uses an infrared camera to detect and locate tumours by observing temperature anomalies on the breast skin surface. These anomalies can be caused by a tumour's high metabolic heat generation and blood perfusion rate. This technique can be used as an adjoint method to mammography in diagnosing tumours in dense breasts, common in women younger than 40 years. A parameter that influences the accuracy of the diagnosis is the thermal contrast since a decrease in its value makes it harder to observe the temperature anomalies. The purpose of this study is to investigate the thermal contrast's impact on the prediction errors of a breast tumour's size and location. A 3D hemispherical breast model with different tissue layers was built to compute the steady state and transient surface temperature profiles. A neural network was used to solve the inverse heat problem and estimate the size and location of the tumours. In those simulations, the location and size of the tumours were changed, with the 625 generated temperature profiles being used to train a neural network developed on MATLAB. The neural network was trained with surface temperature profiles obtained under passive and dynamic thermography conditions. A comparison between the estimates provided by each type of thermography was made. The estimates exhibited high correlation coefficients and strong linear relationships with the real values. An increase in thermal contrast improved the accuracy of all estimated parameters due to higher surface temperature variations. Deep-seated tumours showed no significant estimation error reduction in both types of thermography. The best estimates for parameters x, y and z were obtained by using dynamic thermography. The estimated radius showed the same error for both types of thermography, indicating that the increase in surface temperature variations was small in this case.*

Keywords: *breast cancer, inverse heat conduction problem, thermography, deep learning.*

1. INTRODUCTION

Breast cancer is the most diagnosed and leading cause of cancer death among women worldwide, accounting for 24.51% (2,261,419 cases) of diagnoses and 15.47% (684,996 cases) of deaths in 2020 (WHO, 2023). In Brazil, it is expected to account for 20.29% (73,610 cases) of diagnoses among women in 2023 (INCA, 2022). Mammography is the most widely employed screening method for diagnosing breast cancer. However, it has limitations, such as the emission of ionizing radiation, the discomfort of compression, and low effectiveness for dense and surgically implanted breasts. To improve detection efficiency, thermography has been used as an adjoint method to mammography (Bezerra *et al.*, 2013).

Infrared thermography is a non-invasive and cost-effective screening method that employs an infrared camera to measure the skin surface temperature profile of the breast. A tumour has accelerated growth and a high metabolic rate, sustained by forming new blood vessels (angiogenesis). The heat generated can reach the surface, causing a spike in the temperature profile (Mashekova *et al.*, 2022; Gonzalez-Hernandez *et al.*, 2019).

Two types of thermography can be used for medical screening and diagnosis: passive thermography, where the temperatures are measured when the patient is acclimatised in room conditions, and dynamic thermography, where hyperthermia (heating stress) or hypothermia (cooling stress) is applied on the tissue, with the temperatures being measured during thermal recovery (Gomboc *et al.*, 2021). In dynamic thermography, the applied thermal stress enhances thermal contrast, the temperature difference between cancerous and healthy tissue, which improves the sensitivity and effectivity of the diagnosis, especially for small and deep-seated tumours (Zhou and Herman, 2018).

Previous studies coupled thermography to inverse problems, with tumour parameters such as size, location, and metabolic rate estimated from surface temperature profiles employing different computational modelling techniques.

Mitra and Balaji (2010) used an artificial neural network to estimate the location and the radius of a breast cancer tumour. A hemispherical breast model was employed to obtain the temperature profiles used as training data for the neural network. When the temperature profiles with no noise and constant heat generation were used, the location and radius of the tumour had accuracies of 90 and 95%, respectively. With a variable heat generation, the tumour's location and radius had accuracies of 88 and 98%, respectively. The accuracy of the estimated parameters was reduced when noise was added to the temperatures.

Das and Mishra (2014) used a curve fitting technique with Gaussian fit to estimate the location and size of a breast cancer tumour from temperature profiles. The finite volume method was used to solve Pennes equation and obtain the temperature profiles. Tumour size and location presented maximum errors of 4.167% and 7.7%, respectively.

Saniei *et al.* (2016) trained an artificial neural network with the simulated temperature profiles obtained by employing a hemispherical breast model. The neural network estimated the size and depth of tumours in thermograms of histologically confirmed breast cancer patients. Gravity-induced changes in breast geometry and different tumour shapes reduced the estimated depth accuracy.

Hatwar and Herman (2017) used an inverse heat transfer problem to estimate a tumour's radius, depth, and blood perfusion rate from the temperatures of a section of the surface. A hemispherical breast model was used to obtain temperature profiles. The Levenberg-Marquardt algorithm was employed to solve the inverse problem. The blood perfusion rate couldn't be estimated with steady-state temperatures. The estimated parameters presented a lower accuracy for deep-seated tumours.

Bezerra *et al.* (2020) estimated breast and tumour tissue's thermal conductivity and blood perfusion rate by solving an inverse heat transfer problem with sequential quadratic programming. In addition, an empirical correlation between breast thermal conductivity and patient age was defined. The temperatures provided by the numerical model were close to the experimental measurements. The thermal conductivity provided by the empirical correlation generated more accurate temperature profiles than the one encountered in the literature.

Majdoubi *et al.* (2021) employed a feedforward neural network to estimate the location and the radius of a breast cancer tumour. The neural network was trained with surface temperature profiles and isotherms provided by a numerical model. The z-coordinate of the tumour presented the best estimates, with the y-coordinate showing a larger scatter than the other parameters. The estimated parameters accuracy decreased for tumours smaller than 0.5 cm, especially when embedded in large breasts.

In this work, a feedforward neural network developed on MATLAB will be used to estimate the size and location of breast tumours based on the skin surface temperature profiles of a 3D hemispherical breast model built on COMSOL Multiphysics. The numerical analysis will be carried out under passive and dynamic thermography conditions (hypothermia) to analyse the influence of the thermal contrast on the estimates.

2. METHODOLOGY

2.1 Mathematical and physical model

In this study, the human breast is modelled as a 3D hemispherical domain composed of five tissue layers: skin, fat, tumour, gland, and muscle, as shown in Figure 1. The location and size of the tumour are determined by coordinates x, y, z, and the radius (r). Tumour depth (z) is measured from the top point of the breast surface to the tumour centre, while coordinates x and y are measured from the reference line on the left side. Each layer has its thermophysical properties, which are shown in Table 1.

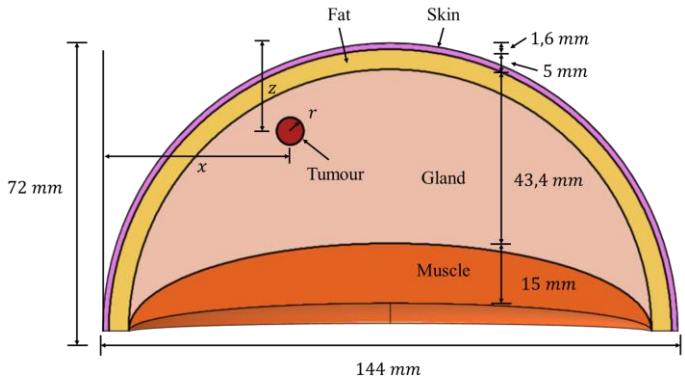

Figure 1. x-z cutting plane in the centre of the breast model's y-axis.

Table 1. Thermophysical properties of each tissue layer adapted from Zhou and Herman (2018) and Figueiredo *et al.* (2020).

Tissue	ρ (kg/m^3)	c (J/kg˚C)	k (W/m˚C)	ω_b (1/s)	Q_m (W/m^3)
Skin	1200	3318	0.432	0.00071	345.1
Fat	930	2674	0.210	0.00008	400.0
Gland	1050	3770	0.480	0.00054	700.0
Muscle	1100	3800	0.480	0.00270	700.0
Tumour	1050	3852	0.480	0.00630	65400

The Pennes equation, as described in Eq (1), models heat transfer in living tissues, coupling the heat conduction through tissue layers, convection generated by the temperature difference between tissue and blood, and metabolic heat generation (Pennes, 1948).

$$\rho_i c_i \frac{\partial T_i}{\partial t} = k_i \nabla^2 T_i + \omega_{b,i} \rho_b c_b (T_b - T_i) + Q_{m,i} \tag{1}$$

where i represents the breast tissue layers, muscle (i=1), gland (i=2), fat (i=3), skin (i=4) and tumour (i=5). The parameters ρ_i, c_i, T_i, t, k_i, $\omega_{b,i}$, and $Q_{m,i}$ are the specific mass, specific heat, temperature, thermal conductivity, blood perfusion rate, and metabolic heat generation rate of each tissue layer, respectively. The values of blood's specific mass (ρ_b), specific heat (c_b), and temperature (T_b) were 1060 kg/m^3, 3770 J/kg˚C, and 37 ˚C, respectively.

The constant temperature and convection boundary conditions applied in the breast model are shown in Figures 2a and 2b, with the heat convection coefficient (h), ambient temperature (T_∞), and hypothermia temperature (T_{hp}) corresponding to 5 W/m^2˚C, 21 ˚C, and 15 ˚C, respectively.

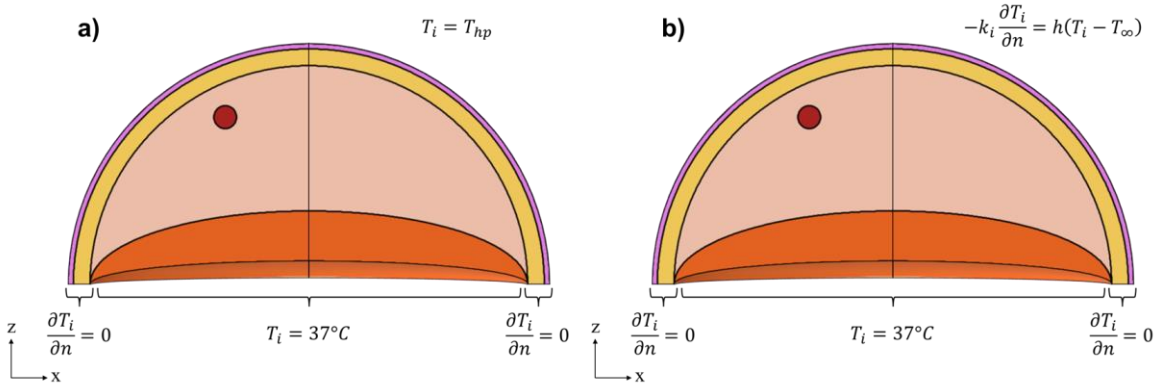

Figure 2. Breast model with a) constant temperature boundary and b) heat convection boundary.

In passive thermography conditions, a heat convection boundary was applied on the breast skin surface, while on the lower surface, a constant temperature of 37 ˚C was maintained on the muscle layer, with two adiabatic walls placed on the horizontal adjacent layers. In dynamic thermography conditions, the breast skin surface was maintained at hypothermia temperature for 1200 s, with a heat convection boundary applied after 1200 s and up to 5400 s. Lower surface boundaries were the same as in passive thermography.

2.2 Numerical simulation

The bioheat transfer model and its boundary conditions were solved using the finite element software COMSOL Multiphysics. A coarse level of refinement was used to generate a different mesh for each breast model, with the number of elements and nodes in the computational domain automatically determined by the mesh generator.

An algorithm in Java was developed in the COMSOL Multiphysics Application Builder to randomly change the tumour's location and radius for each case, creating six datasets, three for each type of thermography, composed of 625 skin surface temperature profiles. Spherical tumours with radii of 0.35 - 0.50 cm were generated inside the gland tissue layer within intervals of 5.7 - 8.7 cm for coordinates x and y and depths of 1.7 - 2.2 cm, 2.2 - 2.7 cm and 2.7 - 3.2 cm. Healthy breast surface temperatures under passive and dynamic thermography conditions were obtained by solving the direct problem without a tumour for both cases.

A total of 137 points were applied on the breast skin surface to measure the temperatures, as shown in Figure 3. The time step employed during thermal recovery was 60 s, generating 71 temperature profiles. In passive thermography, only one temperature profile was generated.

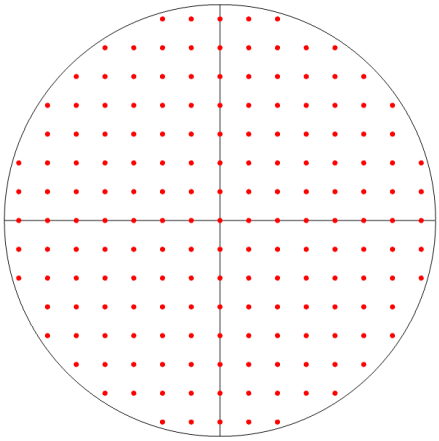

Figure 3. Points on the breast surface.

Another algorithm developed on MATLAB was employed to extract the thermal contrast of each temperature profile while organising them to be used in the training phase of a feedforward neural network. The temperatures obtained under dynamic and passive thermography conditions were used to train the same neural network separately. To compare and analyse their estimates. Only the temperature profiles with the highest thermal contrasts were selected from the dynamic thermography datasets and used in the training phase.

2.3 Multilayer perceptron

A multilayer perceptron is a type of neural network whose input and output layers are connected to a set of one or more intermediate (hidden) layers that interfere in the relationship between input and output in a useful way. Each node is called a neuron, an information processing unit composed of weights (w_{ji}), the strength of each connection, biases (b_j), responsible for decreasing or increasing the input value in the activation function, adder, which sums all inputs (x_i) adjusted by the weights and biases, and activation function (f), which limits the amplitude of the output (y_j). Equation (2) describes the mathematical relationship between the inputs and outputs of a neuron (Haykin, 2009).

$$y_j = f\left(\sum_{i=1}^{n} w_{ji}x_i + b_j\right) \tag{2}$$

where i, n, and j are the input's number, the total number of inputs, and the node's number, respectively.

In this work, a linear activation function, commonly used in the output when the target is a real value, was employed in the output layer, with a sigmoid activation function, used when calculations are to be interpreted as probabilities, being used in the hidden layers, each described in Eq (3) and Eq (4), respectively (Aggarwal, 2018).

$$f(x) = x \tag{3}$$

$$f(x) = \frac{1}{1+e^{-x}} \tag{4}$$

The weights and biases were updated by the Levenberg Marquardt backpropagation algorithm. During training, an input is propagated throughout the neural network, the difference between achieved and targeted values is propagated from output to input, and weights and biases are updated accordingly.

The feedforward multilayer perceptron employed to solve the inverse problem was developed on MATLAB, having an input layer with 137 inputs, three hidden layers with 24, 12 and 6 neurons, and an output layer with four outputs, as shown in Figure 4. The input data comprised 625 temperature profiles with the size and location of their respective tumours. The data was divided into 80% for training and 20% for testing. The training and estimation process of the neural network was repeated six times for each studied case, and the means of the correlation coefficient and absolute error of the estimates were calculated.

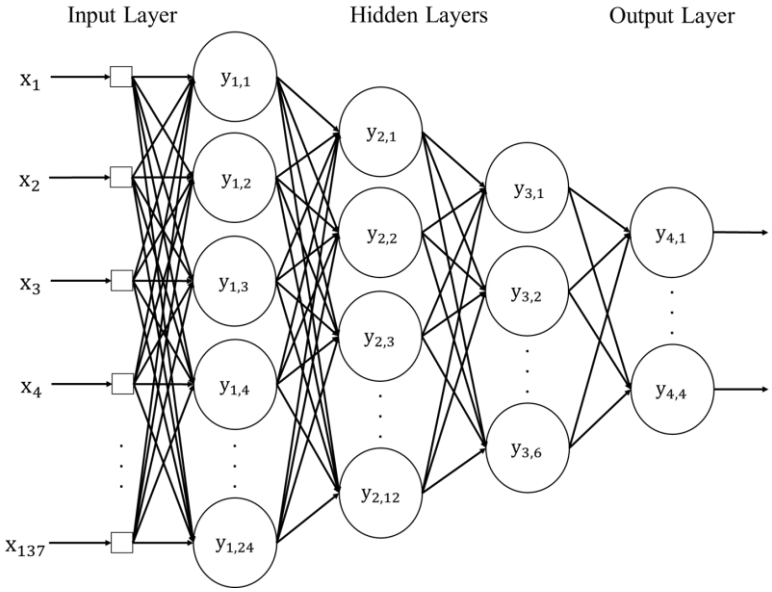

Figure 4. Schematic of the developed neural network.

3. RESULTS AND DISCUSSIONS

Table 2 shows the mean correlation coefficients and mean absolute errors of the estimated parameters for various conditions. The mean correlation coefficients were approximately the same for both types of thermography and all thermal contrast intervals, indicating a strong linear relationship between estimated and real parameters in all cases. The results also show that an overall increase in thermal contrast reduced the prediction errors. However, for deep-seated tumours, none of the parameters showed a significant improvement. This suggests that the surface temperature variations caused by changes in the tumour's size and location were too small to be differentiated by the neural network.

Table 2. Correlation and mean absolute error of the estimates under various conditions.

Type of thermography	Thermal contrast interval (˚C)	Depth Interval (cm)(1)	Mean Correlation	Mean absolute error of x (cm)	Mean absolute error of y (cm)	Mean absolute error of z (cm)	Mean absolute error of r (cm)
Passive	0.356-0.047	1.700-2.200	0.999	0.0024	0.0020	0.0030	0.0006
	0.204-0.026	2.200-2.700	0.999	0.0031	0.0031	0.0041	0.0015
	0.116-0.015	2.700-3.200	0.999	0.0031	0.0032	0.0048	0.0016
Dynamic	0.703-0.075	1.700-2.200	0.999	0.0008	0.0007	0.0017	0.0006
	0.361-0.037	2.200-2.700	0.999	0.0016	0.0015	0.0036	0.0015
	0.186-0.020	2.700-3.200	0.999	0.0017	0.0017	0.0041	0.0016

(1)bigger values correspond to deeper tumours

The estimated x, y and z errors were smaller when dynamic thermography was used, which can be related to an increase in surface temperature variations, highlighting the changes in the temperature profiles and making them easier to differentiate. The tumour's estimated radius presented the same errors for both types of thermography, suggesting that the increase in temperature variations caused by dynamic thermography wasn't significant in this case.

The estimates of x and y showed close errors since both were defined in the same interval and caused analogous temperature variations in the skin surface profiles. In dynamic thermography, these parameters showed an error reduction of about 200%, indicating a significant improvement in the temperature profiles.

The estimates of z and r were close to the real values since these parameters determine if the heat generated by the tumour can reach the surface, with small variations in each of them causing significant changes in the temperature profiles and their thermal contrast.

Figures 5a, 5b, 5c and 5d show the parity plots of x, y, z and r under dynamic thermography conditions in a 2.2-2.7 cm depth, respectively. The estimated parameters exhibited high correlation coefficients, reflected in strong linear relationships with the real values, showing that the neural network can accurately predict a tumour's size and location using only surface temperature profiles obtained under dynamic thermography conditions.

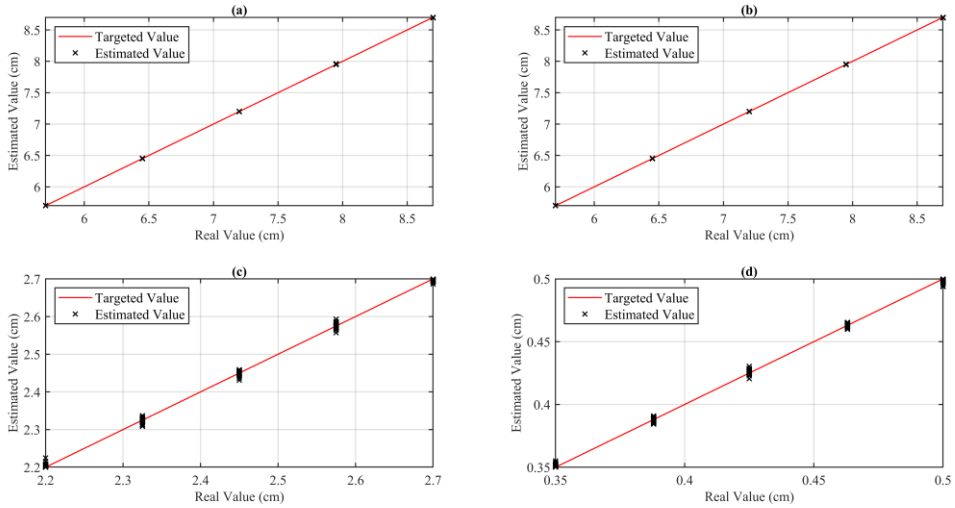

Figure 5 - Parity plots of a) x, b) y, c) z and d) r under dynamic thermography and within a 2.2-2.7 cm depth interval.

Figures 6a, 6b, 6c and 6d show the absolute error plots of x, y, z and r under dynamic thermography conditions in a 2.2-2.7 cm depth, respectively. The maximum absolute errors observed in x and y were 0.0114 and 0.0117 cm, respectively. However, both had a mean absolute error of 0.0012 cm due to an overall low error of the estimates. The mean and maximum absolute errors for the z-coordinate were 0.0027 cm and 0.0274 cm, respectively, while for r, they were 0.0010 cm and 0.0061 cm.

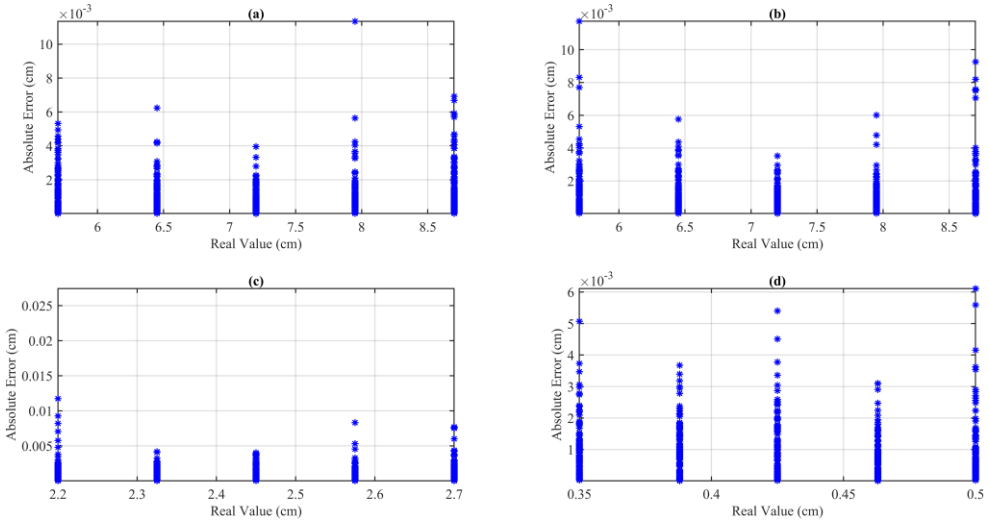

Figure 6 – Absolute error plots of a) x, b) y, c) z and d) r under dynamic thermography and within a 2.2-2.7 cm depth interval.

Figures 7a, 7b, 7c and 7d show the thermal contrast plots of x, y, z and r under dynamic thermography conditions in a 2.2-2.7 cm depth, respectively. The temperature profiles with the lowest thermal contrast were the ones closer to the breast centreline and with the largest depths and smallest radii. The heat generated by the tumour has more difficulty reaching the surface when the distance is larger, so increasing the depth reduces thermal contrast. The same occurs when the tumour is closer to the centreline since it increases the distance between the tumour and the surface. Additionally, small tumours have low volumetric heat generations and blood perfusion rates, negatively impacting thermal contrast.

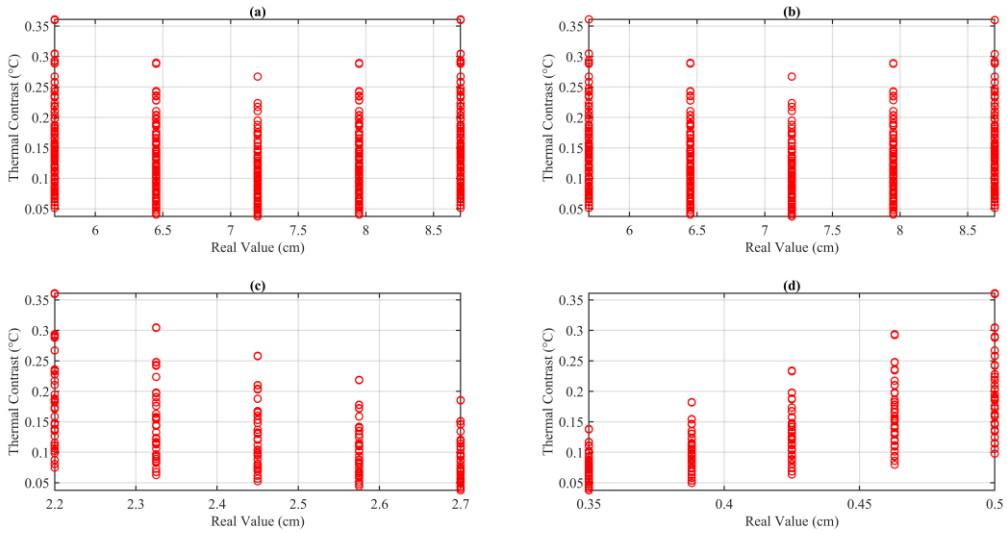

Figure 7 – Thermal contrast plots of a) x, b) y, c) z and d) r under dynamic thermography and within a 2.2-2.7 cm depth interval.

The results show that high thermal contrast temperature profiles can have larger estimation errors than others with a lower thermal contrast in the same dataset, indicating that the thermal contrast of a temperature profile does not determine the error of its estimate, so the focus should be on increasing the overall thermal contrast of the dataset to improve the estimation accuracy of all cases.

4. CONCLUSION

In this work, a 3D hemispherical breast model was used to generate six datasets of surface temperature profiles to train a neural network and investigate the influence of thermal contrast on the estimates. The commercial software COMSOL Multiphysics was used to solve Pennes bioheat equation. A feedforward neural network was developed on MATLAB to estimate the size and location of breast tumours. A comparison was made between the accuracy of estimates obtained using passive and dynamic thermography.

The high correlation coefficients indicate that the neural network can accurately predict the tumour's parameters using only surface temperature profiles. Dynamic thermography provided the best estimates of x, y and z, which can be related to an increase in surface temperature variations. The estimated radius errors were the same for both types of thermography, indicating a small difference in temperature variations between each method in this case.

An increase in the overall thermal contrast of a dataset reduced the errors of all estimated parameters except for deep-seated tumours. However, the thermal contrast of an individual temperature profile does not determine its estimate error, with some high thermal contrast temperature profiles providing less accurate estimates than lower thermal contrast ones in the same dataset.

5. ACKNOWLEDGEMENTS

This study was funded by the Coordination for the Improvement of Higher Education Personnel (CAPES) – Brazil.

6. REFERENCES

Aggarwal, C. C, 2018. *Neural Networks and Deep Learning: A Textbook*. Springer Nature Switzerland AG, *Cham*.

Bezerra, L. A., Oliveira, M. M., Rolim, T. L., Conci, A., Santos, F. G. S., Lyra, P. R. M., and Lima, R. C. F., 2013. "Estimation of breast tumor thermal properties using infrared images". *Signal Processing*, Vol. 93, pp. 2851-2863.

Bezerra, L. A., Ribeiro, R. R., Lyra, P. R. M., and Lima, R. C. F., 2020. "An empirical correlation to estimate thermal properties of the breast and of the breast nodule using thermographic images and optimization techniques". *International Journal of Heat and Mass Transfer*, Vol. 149, pp. 119215.

Das, K. and Mishra, S. C., 2014. "Non-invasive estimation of size and location of a tumor in a human breast using a curve fitting technique". *International Communications in Heat and Mass Transfer*, Vol. 56, pp. 63-70.

Figueiredo, A. A. A., Fernandes, H. C., Malheiros, F. C., and Guimaraes, G., 2020. "Influence analysis of thermophysical properties on temperature profiles on the breast skin surface". *International Communications in Heat and Mass Transfer*, Vol. 111, pp. 104453.

Gomboc, T., Iljaž. J., Wrobel, L. C., Hriberšek, M., and Marn, J., 2021. "Design of constant temperature cooling device for melanoma screening by dynamic thermography". *Engineering Analysis with Boundary Elements*, Vol. 125, pp. 66-79.

Gonzalez-Hernandez, J.-L., Recinella, A. N., Kandlikar, S. G., Dabydeen, D., Medeiros, L., Phatak, P., 2019. "Technology, application and potential of dynamic breast thermography for the detection of breast cancer". *International Journal of Heat and Mass Transfer*, Vol. 131, pp. 558-573.

Hatwar, R. and Herman, C, 2017. "Inverse method for quantitative characterisation of breast tumours from surface temperature data". *International Journal of Hyperthermia*, Vol. 33, pp. 741-757.

Haykin. S., 2009. *Neural networks and learning machines*. Pearson Education, Inc, New Jersey.

INCA, 2023. Estimate 2023 – Cancer Incidence in Brazil (in Portuguese). Instituto Nacional do Câncer, Rio de Janeiro. https://www.inca.gov.br/sites/ufu.sti.inca.local/files//media/document//estimativa-2023.pdf. Accessed 30 May 2023.

Majdoubi, J., Iyer, A. S., Ashique, A. M., Perumal, D. A., Mahrous, Y. M., Rahimi-Gorji, M., and Issakhov, A., 2021. "Estimation of tumor parameters using neural networks for inverse bioheat problem". *Computer Methods and Programs in Biomedicine*, Vol. 205, pp. 106092.

Mashekova, A., Zhao, Y., Ng, E. Y. K., Zarikas, V., Fok, S. C., and Mukhmetov, O., 2022. "Early detection of the breast cancer using infrared technology – A comprehensive review". *Thermal Science and Engineering Progress*, Vol. 27, pp. 101142.

Mitra, S. and Balaji, C, 2010. "A neural network based estimation of tumour parameters from a breast thermogram". *International Journal of Heat and Mass Transfer*, Vol. 53, pp. 4714-4727.

Pennes, H. H., 1948. "Analysis of tissue and arterial blood temperatures in the resting human forearm". *Journal of Applied Physiology*, Vol. 1, pp. 93-122.

Saniei, E., Setayeshi, S., Akbari, M. E., and Navid, M., 2016. "Parameter estimation of breast tumour using dynamic neural network from thermal pattern". *Journal of Advanced Research*, Vol. 7, pp. 1045-1055.

WHO, 2020. Cancer Today. https://gco.iarc.fr/today/online-analysis-table?v=2020&mode=cancer&mode_population=continents&population=900&populations=900&key=asr&sex=2&cancer=39&type=0&statistic=5&prevalence=0&population_group=0&ages_group%5B%5D=0&ages_group%5B%5D=17&group_cancer=1&include_nmsc=0&include_nmsc_other=1. Accessed 30 May 2023.

Zhou, Y. and Herman, C., 2018. "Optimization of skin cooling by computational modeling for early thermographic detection of breast cancer". *International Journal of Heat and Mass Transfer*, Vol. 126, pp. 864-876.

7. RESPONSIBILITY NOTICE

The authors are the only ones responsible for the printed material included in this paper.